Chemical Engineering Journal 204–206 (2012) 258–263

Contents lists available at SciVerse ScienceDirect

Chemical Engineering Journal

journal homepage: www.elsevier.com/locate/cej

Synthesis, characterization and adsorption properties of superparamagnetic polystyrene/Fe_3O_4/graphene oxide

Jinfeng Wang [a], Bin Tang [a], Takuya Tsuzuki [a,*], Qingtao Liu [b], Xueliang Hou [a], Lu Sun [a,*]

[a] Australian Future Fibres Research & Innovation Centre, Institute for Frontier Materials, Deakin University, Geelong, Victoria 3217, Australia
[b] Drug Delivery, Disposition and Dynamics, Monash Institute of Pharmaceutical Sciences, Monash University, 381 Royal Pde, Parkville, Victoria, Australia

HIGHLIGHTS

- Novel PS@Fe_3O_4@GO nanoparticles were fabricated using a self-assembly method.
- PS@Fe_3O_4@GO exhibited a higher loading of Fe_3O_4 than reported GO@Fe_3O_4 systems.
- PS@Fe_3O_4@GO exhibited better magnetic responsivity than reported GO@Fe_3O_4 systems.
- The layered structure retained efficient surface area of GO to load organic molecules.

GRAPHICAL ABSTRACT

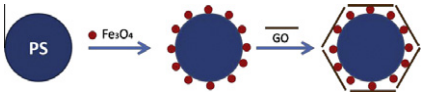

ARTICLE INFO

Article history:
Received 16 April 2012
Received in revised form 12 July 2012
Accepted 18 July 2012
Available online 28 July 2012

Keywords:
Superparamagnetic spheres
Electrostatic self-assembly
Graphene oxide
Drug delivery

ABSTRACT

Core–shell structured polystyrene (PS)-Fe_3O_4-graphene oxide (GO) composite nanoparticles were synthesized by sequentially depositing Fe_3O_4 nanoparticles and GO sheets onto the carboxyl functionalized PS template nanoparticles through electrostatic interactions. Morphologies of the composite nanoparticles were studied by both scanning electron microscopy and transmission electron microscopy, while their structures and chemical components were examined via Fourier transform infrared spectroscopy, Raman spectroscopy and X-ray photoelectron spectroscopy. The data confirmed the coexistence of PS, Fe_3O_4 and GO with a core–shell structure in the composite. The obtained PS@Fe_3O_4@GO nanoparticles possess excellent magnetic responsivity to externally applied magnetic field and can also form stable dispersion upon the removal of magnetic field. The study on the loading capacity of model molecule Rhodamine B (RhB) indicated the possibilities of using PS@Fe_3O_4@GO nanoparticles in targeted drug delivery applications.

1. Introduction

Graphene, a free standing two dimensional crystal with one-atom thickness, has attracted much attention because of its unique properties, such as remarkable electronic properties, superlative mechanical strength (Young's modulus, 1100 GPa) [1], unparalleled thermal conductivity (5000 W/m/K) [2] and high planar surface area (calculated value, 2630 m^2/g) [3]. The large surface area can be used for the immobilization of a large number of substances including dyes, metals, bio-molecules, and drugs. Functionalized graphene nanosheets are biocompatible with no obvious toxicity [4] and their composites have been used for drug delivery, photothermal therapy and magnetic resonance imaging [5,6]. GO has also been used for adsorbing dye from wastewater discharged from the textiles, printing, and tanning industries [7]. Although improving the loading efficiency is critical in molecule adsorption research, site-directed is also very important for increasing drug efficacy and facilitating dye removal.

One of the promising site-directed methods is to use magnetic nanoparticles in the molecule-loading nanocomposites. In fact, as an important family of advanced nanomaterials, magnetic

* Corresponding authors. Tel.: +61 3 5227 3205; fax: +61 3 5227 2539 (T. Tsuzuki), tel.: +61 3 5227 3247; fax: +61 3 5227 2539 (L. Sun).
E-mail addresses: takuya.tsuzuki@deakin.edu.au (T. Tsuzuki), lu.sun@deakin.edu.au (L. Sun).

1385-8947/$ - see front matter © 2012 Elsevier B.V. All rights reserved.
http://dx.doi.org/10.1016/j.cej.2012.07.087

nanocomposites have gained much attention, due to their ability to realize both magnetic targeting and effective magnetic separation to selectively capture the objects of interest from a complex mix of substances [8].

Yang et al. prepared a hybrid material consisting of GO and Fe_3O_4 nanoparticles using a chemical deposition method and used to bind doxorubicin hydrochloride (DXR) for targeted drug delivery [9]. Magnetic Fe_3O_4@GO composites were also synthesized for dye removal from aqueous media [10]. However, there are two major shortcomings of the Fe_3O_4@GO adsorbent. One is that the adsorption of Fe_3O_4 nanoparticles and molecules was mutually exclusive on GO sheets, which limited the amount of molecules that could be loaded on the surface of GO nanosheets in the presence of Fe_3O_4 nanoparticles. The other problem is that the strong hydrophilic property of GO enables the GO@Fe_3O_4 well dispersed in water, which is a disadvantage in promoting magnetic separation.

One of the effective approaches to overcome these limitations is to use a spherical nano-carrier core to load as much as Fe_3O_4 nanoparticles and then coat GO nanosheets on the very outside of the composite nanoparticles. This layered structure not only increases the amount of Fe_3O_4 nanoparticles in the composite, but also provides a high surface area of GO nanosheets for further molecule loading. More importantly, the spherical shape as opposed to thin-sheet like morphology could significantly reduce the viscosity of the carrier@Fe_3O_4@GO suspension system, compared to that of GO@Fe_3O_4, enabling the fast response of the composite nanoparticles to external magnetic field under various pH conditions.

In this article, spherical GO composite nanoparticles with the layered structure were fabricated and their potential as a drug-delivery system was studied. Polymeric latex spheres were used as an ideal carrier of GO and Fe_3O_4 nanoparticles for its large surface area, high chemical stability, arbitrary functional groups on the surface, low cost and good dispersion stability in aqueous/non-aqueous solutions [11]. Fe_3O_4 nanoparticles were coated on carboxyl functionalized PS latex spheres and then GO was coated to form an outside shell (PS@Fe_3O_4@GO). This GO-based sandwich structure can easily respond to external magnetic field and can be well redispersed into water upon the removal of magnetic field. It also displayed an improved responsivity to an external magnetic field compared to previously reported GO@Fe_3O_4 system. The capacity of PS@Fe_3O_4@GO to load organic molecules was also investigated. These properties make PS@Fe_3O_4@GO a good promising material for targeted drug delivery applications.

2. Experimental sections

2.1. Materials

Tetraethylorthosilicate (TEOS), potassium persulfate (KPS) and graphite were obtained from Sigma–Aldrich. Styrene (St) and acrylic acid (AA) were obtained from Sigma–Aldrich and both of them were purified by distillation under reduced pressure before use. Ferric chloride hexahydrate, ferrous chloride tetrahydrate, ammonium hydroxide, sodium hydroxide (NaOH) and potassium permanganate were purchased from Chem-supply Pty Ltd. (Gillman, Australia).

2.2. Synthesis of PS@Fe_3O_4@GO composite nanoparticles

2.2.1. Synthesis of Fe_3O_4 nanoparticles

Fe_3O_4 nanoparticles were synthesized according to the Massart's method [12]. Under vigorous mechanical stirring, 20 mL of a freshly prepared aqueous mixture of ferric chloride hexahydrate (2.70 mM) and ferrous chloride tetrahydrate (1.35 mM) was added to an ammonium solution (110 mL, 1.5 M) under N_2 protection. After 30 min, the precipitate was isolated from the solution by magnetic decantation and washed three times with water.

2.2.2. Synthesis of PS nanoparticles

Carboxylic PS latex was prepared by soap free emulsion polymerization of styrene (St) with acrylic acid (AA) [13]. Typically, 100 mL water, 0.12 g $NaHCO_3$, 5 mL St and 0.5 mL AA were added into a three-necked flask fitted with a reflux condenser and a mechanical stirrer. KPS served as the initiator and no emulsifier was used in the polymerization. The reaction was carried out under a N_2 atmosphere at 70 °C for 12 h with mechanical stirring at 300 rpm. The resulting latex was purified by three centrifugation/dispersion cycles in water.

2.2.3. Synthesis of GO suspension

GO was prepared using a modified Hummers method [14]. Briefly, 10 g graphite flake and 7.5 g sodium nitrate were added to 300 mL of sulfuric acid (98%), and then 40 g of potassium permanganate was added to the reaction slowly in 1 h. The mixture was stirred at room temperature for 3 days. 1 L of hydrogen peroxide solution (1% in water) was then added into the mixture. Subsequently, the mixture was filtered and washed with deionized water until pH became 7. The resulting black cake was re-dispersed in de-ionized water to give a dark brown dispersion, which was subjected to dialysis for one week to remove the residual salts and acids. And the brown suspension was dried at 40 °C under vacuum. GO suspension was then obtained by sonicating the as-prepared black solid in water under ambient condition for 30 min, followed by centrifugation at 3000 rpm for 30 min to remove the unexfoliated GO. The resulting homogenous brown dispersion was tested to be stable for several months and used for assembling.

2.2.4. Synthesis of PS@Fe_3O_4 composite nanoparticles

The PS latex and Fe_3O_4 nanoparticles were washed with an aqueous solution with a pH value of 3, and then dispersed in the same solution by ultrasonic treatment. 1 mL PS (10 mg/mL) dispersion was added to a 5 mL dispersion of Fe_3O_4 nanoparticles (6 mg/mL) under vigorous stirring. After 6 h, the hetero-aggregates were separated from the solution by centrifugation and washed several times with an acidic aqueous solution (pH = 3, adjusted with HCl) to remove non-adsorbed Fe_3O_4 nanoparticles, and then PS@Fe_3O_4 was dispersed in water (pH = 7) for the next step of assembly.

2.2.5. Synthesis of PS@Fe_3O_4@GO composite nanoparticles

20 mL of GO aqueous dispersion (0.5 wt.%) was added into the above PS@Fe_3O_4 aqueous dispersion. The mixed dispersion was shaken gently for 6 h, and the final product was separated from the host liquid by a magnet, and washed three times to remove non-adsorbed GO nanosheets.

2.2.6. Rhodamine B (RhB) loading onto PS@Fe_3O_4@GO

The obtained PS@Fe_3O_4@GO powder was dispersed into RhB aqueous solution (3 mL, 0–150 ppm) at a concentration of 2 mg/mL. The dispersion was stirred in the dark at room temperature for 24 h. The composite was washed with water using a magnet as a collector. The washing cycle was repeated until the supernatant became colorless. The washed PS@Fe_3O_4@GO with loaded RhB was redispersed in water and used for ultraviolet–visible (UV–vis) light spectroscopic characterization. At the same time, all the supernatants collected from each washing cycles were pooled together, and the amount of the free RhB in the supernatant was determined by UV–vis spectrophotometer at 543 nm. RhB loading capacity (LC) of the composite was estimated indirectly

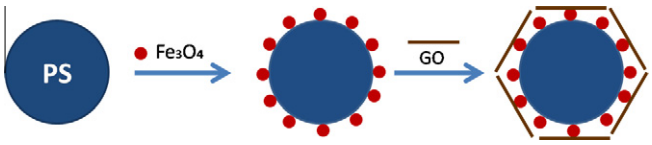

Scheme 1. Synthesis procedure of PS@Fe_3O_4@GO nanoparticles.

by determining the amount of the unbound RhB in the supernatant according to the following equation.

$$LC_{\text{indirect}}(\%) = \frac{\text{total RhB used} - \text{RhB in supernatant}}{\text{total PS@Fe}_3\text{O}_4\text{@GO weight}} \times 100$$

2.3. Characterization

The morphologies and structures of the samples were studied by atomic force microscopy (AFM, Asylum Research Cypher) and transmission electron microscopy (TEM) using a JEOL-2100 microscope operated at an acceleration voltage of 200 kV. Scanning electron microscopy (SEM) was carried out with a Supra SEM 55VP (Carl Zriss, Germany) microscope. The optical absorption spectra of the samples were obtained using a Varian Cary 3E UV–vis spectrophotometer. Fourier transform infrared (FT-IR) spectra were measured with a Bruker Vertex 70 FT-IR spectrophotometer using the KBr method. Thermal gravimetric analysis (TGA) curves were obtained using a Netzsch STA 407PC with a heating temperature rate of 10 °C min^{-1} under an air atmosphere. Raman spectra were obtained by using a Horiba Jobin Yvon T64000 system. A 532 nm radiation from a 20 mW argon ion laser was used as an excitation source. X-ray photoelectron spectroscopy (XPS) analysis was performed on a Thermo ESCALAB 250 spectrometer with a Mg Kα (1253.6 eV) achromatic X-ray source. The curves of magnetization versus applied magnetic field (M–H) were measured at room temperature using a superconducting quantum interference device (SQUID) magnetometer (Quantum Design Inc.).

3. Results and discussion

Scheme 1 shows a fabrication procedure of PS@Fe_3O_4@GO. The components, i.e., PS nanoparticles, Fe_3O_4 nanoparticles and GO nanosheets were separately synthesized. Then the layers of Fe_3O_4 nanoparticles and GO nanosheets were consecutively deposited on the PS nanocarriers to construct the PS@Fe_3O_4@GO composite. Electrostatic interaction was utilised as the driving force to self-assemble the components. To deposit Fe_3O_4 nanoparticles on PS efficiently, PS template nanoparticles were synthesized with acrylic acid on the surface to endow abundant amount of —COOH functional groups on the surface of PS particles, which could enhance the deposition of Fe_3O_4 on the surface of PS nanoparticles by electrostatic interactions. TEM images show that the obtained Fe_3O_4 nanoparticles have a near uniform size of around 9 nm (Fig. 1a). The SEM image in Fig. 1b confirms that the size of PS particles was around 200 nm with a narrow size distribution.

During the synthesis of PS@Fe_3O_4 composite nanoparticles, HCl was used to adjust the pH value of both Fe_3O_4 and PS aqueous suspensions to be 3. This resulted in the zeta potential of Fe_3O_4 and PS to be 38.1 and −22.7 eV, respectively. After incubation with PS nanoparticles in solution for 6 h under stirring, the Fe_3O_4 nanoparticles were deposited on the surface of PS particles, via the electrostatic attraction between positively charged Fe_3O_4 and negatively charged PS. Fig. 1c shows a SEM image of PS@Fe_3O_4. The particles were spherical in shape. They appeared to have rough surfaces, which is attributed to the fact that the PS@Fe_3O_4 particles were formed by packing many Fe_3O_4 particles on the surface of PS template particles. The average particle size of PS@Fe_3O_4 particles was calculated from several microscopic images taken from different area of the sample. After Fe_3O_4 coating, the average size of magnetic PS beads increased from 200 to 220 nm. This indicates that the thickness of the Fe_3O_4 shell was ~10 nm (which is estimated as half of the increment in the total diameter of the particle after coating process). The estimated shell thickness was nearly the same as the diameter of Fe_3O_4 nanoparticles (~9 nm), indicating

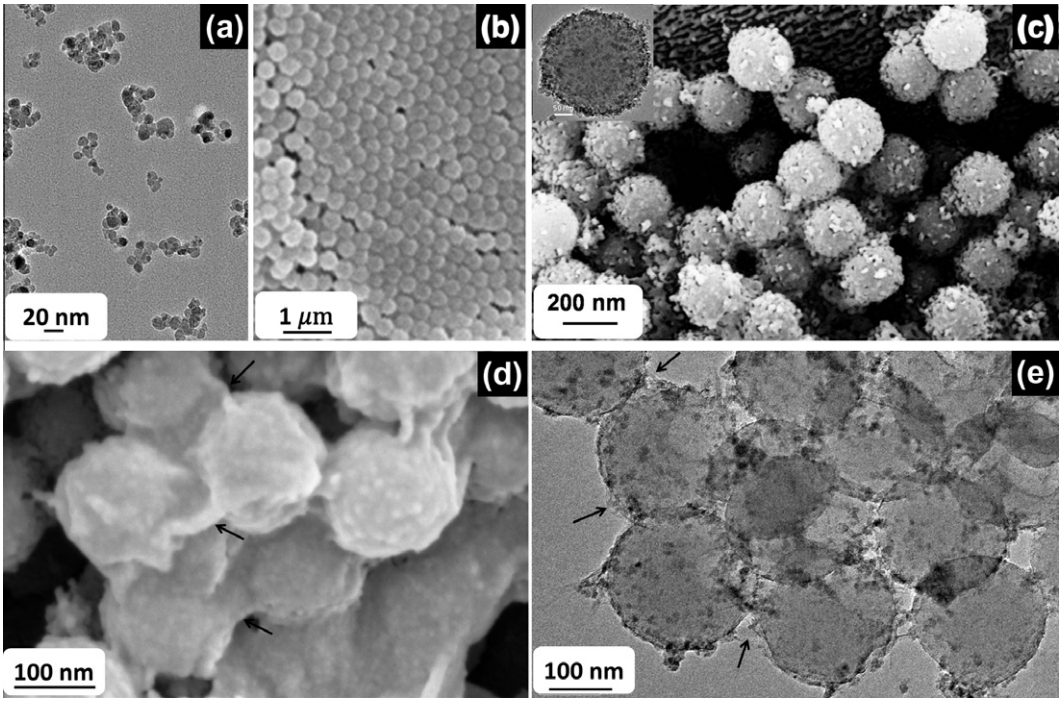

Fig. 1. (a) TEM image of Fe_3O_4 nanoparticles, (b) SEM image of PS nanoparticles, (c) SEM image of PS@Fe_3O_4, inset is the corresponding TEM image of PS@Fe_3O_4, and (d, e) SEM and TEM images of PS@Fe_3O_4@GO, respectively.

that a monolayer of Fe_3O_4 was deposited on the surface of PS nanoparticles. The TEM image of the obtained PS@Fe_3O_4 microspheres (insert of Fig. 1c) shows the dark spots on the PS nanoparticles, which also reveals that the surface of PS nanoparticles was covered by a thin layer of magnetic nanoparticles.

The as-synthesized GO was characterized by AFM and UV–vis absorbance spectroscopy (Fig. S1). The lateral size of the resulting GO sheets ranged from tens of nanometers to hundreds of nanometers (Fig. S1a). An absorbance band at 230 nm appeared in the UV–vis spectrum, which is attributed to characteristic absorption band of GO (Fig. S1b). At pH = 7, GO is negatively charged due to the residual defects such as the carboxyl, hydroxyl and epoxy groups. On the other hand, Fe_3O_4 coated PS spheres are positively charged. Hence the self-assembly of GO on the PS@Fe_3O_4 surface can readily take place by directly absorbing GO nanosheets on PS@Fe_3O_4 nanoparticles through electrostatic interactions. The dispersion stability of the composite after coating with GO in aqueous system was expected to be remarkably improved because of the stronger zeta potential value of GO compared to that of Fe_3O_4 nanoparticles. It was observed that the PS@Fe_3O_4 dispersion became from turbid to stable transparent during the self-assembly process. This is a clear indication of the assembly of GO on the surface of PS@Fe_3O_4 nanoparticles. The morphologies of the obtained PS@Fe_3O_4@GO are shown in Figs. 1d and 1e. It is evident that GO layers were coated on the surface of the PS@Fe_3O_4. Moreover, no free GO was found in the obtained product because only the magnetic materials were collected during the synthesis.

To further confirm the existence of GO in the composite of PS@Fe_3O_4@GO, Raman spectroscopy and XPS of PS@Fe_3O_4@GO composites were carried out. In Raman spectrum (Fig. S2), the two bands at 1350 and 1600 cm^{-1} are assigned to D band and G band of GO, respectively [15–17], which confirmed the presence of GO in the PS@Fe_3O_4@GO composites. The XPS spectra of PS@Fe_3O_4 and PS@Fe_3O_4@GO show the peaks corresponding to C, O and Fe elements (Fig. S3). The high resolution XPS scan of the PS@Fe_3O_4 shows the presence of one main type of carbon bond C═C (284.6 eV). On the other hand, the high resolution XPS spectrum of PS@Fe_3O_4@GO shows two main types of carbon bonds; C═C (284.6 eV) and C═O (286.7 eV) (see supporting information, Fig. S3), which further supports the presence of GO nanosheets on the surface of PS@Fe_3O_4 spheres.

Zeta potential further confirmed the successful fabrication of PS@Fe_3O_4@GO. As illustrated in Table 1, the zeta potential of PS particles at pH = 3 was −22.7 eV, and became 34.8 eV after incubation with Fe_3O_4 nanoparticles, which was close to the zeta potential of Fe_3O_4 nanoparticles. This result indicates that the surface of PS@Fe_3O_4 was mostly dominated by Fe_3O_4 nanoparticles. After incubating with GO sheets at pH = 7, the zeta potential of PS@Fe_3O_4 turned from 23.7 eV to be −31.6 eV which was close to the value of GO nanosheets. The result indicates that most of the PS@Fe_3O_4 particles were coated with GO layers. The interaction among Fe_3O_4, PS and GO was further characterized by FT-IR. The FT-IR spectra of Fe_3O_4, PS, PS@Fe_3O_4 and PS@Fe_3O_4@GO are shown in Fig. 2. For the pristine carboxyl-group functionalized PS, a broad shoulder at 3428 cm^{-1} is attributed to the hydroxyl stretching vibrations of the C—OH groups and the peaks at 1740 and 1700 cm^{-1} are assigned to the C═O stretching vibrations of typical carbonyl and carboxyl groups, which indicates the presence of —COOH functional groups of PS nanoparticles [18]. After coating of PS spheres with Fe_3O_4 nanoparticles, the peak at 1740 cm^{-1} shifted to 1648 cm^{-1} due to the formation of —COO^-, which indicates that coordination interaction existed between the PS spheres and Fe_3O_4 nanoparticles [9]. The coordination interaction was further supported by the appearance of a new peak associated with the stretching vibration of Fe—O bond at higher wavenumbers of 633 cm^{-1} compared to that of 572 cm^{-1} for the stretching mode of Fe—O in Fe_3O_4 nanoparticles [19]. The FT-IR features of GO suggests the presence of oxygen-containing functional groups on GO nanosheets. The FT-IR spectrum of GO shows an absorption band at 1729 cm^{-1} due to the C═O stretching vibration. It also illustrates the appearance of absorption bands corresponding to epoxy C—O (1243 cm^{-1}) and alkoxy C—O (1071 cm^{-1}) groups, while the broad absorption band at 3420 cm^{-1} can be ascribed to the O—H stretching vibration of GO. The observation of those absorption bands is in agreement with the reported data [20,21]. In the PS@Fe_3O_4@GO, the coordination interaction between GO and Fe_3O_4 was expected to exist according to the previous report about GO@Fe_3O_4 [22]. However, it was unable to observe the relevant change in these bands in the spectra of PS@Fe_3O_4@GO. Nonetheless, the results from zeta potential and FT-IR suggest that both electrostatic and coordination interactions among PS, GO and Fe_3O_4 contributed to the formation of the PS@Fe_3O_4@GO composite nanoparticles. Additionally, the loading level of Fe_3O_4 and GO in the composites was determined by TGA (Fig. S4 in supporting information). The loading amount of Fe_3O_4 was found to be around 43.1 wt.% in PS@Fe_3O_4 and 34.4 wt.% in PS@Fe_3O_4@GO (Fig. S4). Assuming that the weight ratio between PS and Fe_3O_4 remained the same before and after the formation of PS@Fe_3O_4@GO, the amount of GO in PS@Fe_3O_4@GO was calculated to be 16.2 wt.%. However, the competitive electrostatic interaction between PS and GO with Fe_3O_4 nanoparticles may cause Fe_3O_4 to peel off from the PS spheres, resulting in a decreased amount of Fe_3O_4 on the surface of PS nanospheres. Therefore, the actual amount of GO in the composite may be slightly less than the calculated value.

The magnetization curve of PS@Fe_3O_4@GO nanoparticles was measured at room temperature, as shown in Fig. 3a. The magnetic hysteresis loops showed S-shaped curves. The remanent magnetization of the sample was −0.24 emu g^{-1}, which is close to 0. The data indicate that PS@Fe_3O_4@GO exhibits a superparamagnetic behavior. The superparamagnetic properties could help prevent

Table 1
Zeta potential of the composites after each step assembly.

Sample	PS		Fe_3O_4		PS@ Fe_3O_4		GO	PS@Fe_3O_4@GO
pH value	3	7	3	7	3	7	7	7
Zeta potential (eV)	−22.7	−33.0	38.1	25.1	34.8	23.7	−34.0	−31.6

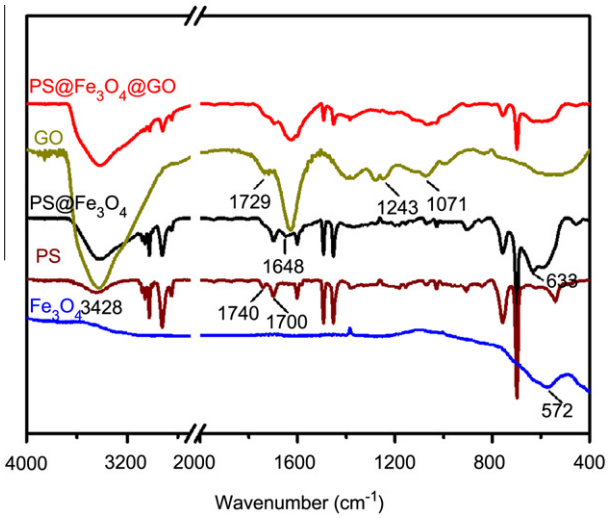

Fig. 2. FT-IR spectra of Fe_3O_4, PS, PS@Fe_3O_4, GO and PS@Fe_3O_4@GO.

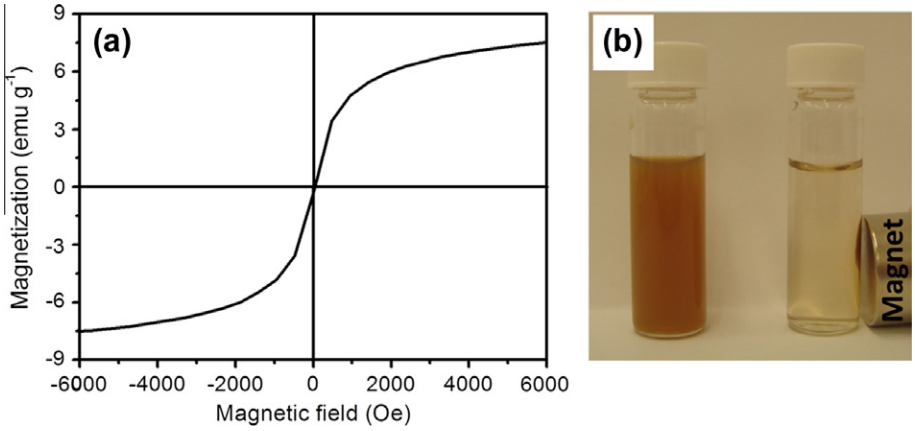

Fig. 3. (a) Magnetization curve of PS@Fe_3O_4@GO hybrid, (b) a photograph represents the magnetic separation of PS@Fe_3O_4@GO from neutral conditions.

the aggregation of the PS@Fe_3O_4@GO when no external magnetic field is applied, which is important for the further applications as targeted drug carriers. The specific saturation magnetization of PS@Fe_3O_4@GO was 7.50 emu g^{-1}, much higher than the value reported for GO@Fe_3O_4, which could be attributed to the relatively higher amount of Fe_3O_4 loaded in the PS@Fe_3O_4@GO composite nanoparticles compared to the reported GO@Fe_3O_4 [9]. Fig. 3b shows the magnetic separation of the PS@Fe_3O_4@GO from the host liquid under pH-neutral conditions. The color of the initial PS@Fe_3O_4@GO was brownish (left-hand side). After application of the external magnetic field, the PS@Fe_3O_4@GO was enriched to the side of the magnet. This demonstrates the possibility of magnetically assisted targeting of the PS@Fe_3O_4@GO under pH conditions similar to biological fluids.

The dispersion stability of PS@Fe_3O_4 at pH = 7 was significantly increased after being coated with GO nanosheets, because of the strongly hydrophilic nature and stronger zeta potential of GO compared to PS@Fe_3O_4 nanoparticles [23]. Fig. 4 shows the images of the behavior of PS@Fe_3O_4@GO under a pH-neutral condition (a), acid conditions (pH 3–4) (b–f) and a basic condition (pH 8–9) (g). The superparamagnetic PS@Fe_3O_4@GO moved slowly under pH-neutral conditions, indicating the good dispersion characteristics in water. However, it congregated immediately after adding one or two drops of HCl (0.5 M) solution and moved readily with the help of an external magnet. The composite nanoparticles can agglomerate under acid conditions through hydrogen bonding interaction [6]. This pH-dependent response to the external magnetic field would be exploitable for the applications as a pH triggered transporter for drug administration. Moreover, as shown in Fig. 4g, the conjugated PS@Fe_3O_4@GO hybrid was re-dispersible into NaOH aqueous solution (pH 8–9) when the external magnetic field is removed. This dispersion stability is consistent with the fact that carboxylic groups on GO become more ionized with increasing pH, resulting in greater sheet electrostatic repulsions. In addition, the stability of the PS@Fe_3O_4@GO composite was monitored under acid conditions. The morphologies of PS@Fe_3O_4@GO maintained after an acid treatment (Fig. S5a). Meanwhile, there was no observable difference in the FT-IR spectra of PS@Fe_3O_4@GO before and after the acid treatment (Fig. S5b). These results indicated that the compositions of PS@Fe_3O_4@GO were stable under the acidic conditions applied in our experiment.

Since GO has sp2-bonded carbon atoms, the GO on the surface of PS@Fe_3O_4@GO will interact with the delocalized π-bonds of organic aromatic compounds and will result in the adsorption of the organic compounds on GO. The high dispersion stability of PS@Fe_3O_4@GO will help maintain its high surface area and assist the adsorption of the organic compounds in the aqueous solution. Thus, PS@Fe_3O_4@GO is expected to be an efficient carrier of aromatic compounds. Herein, a model molecule RhB was used to verify the loading capacity of PS@Fe_3O_4@GO composite nanoparticles. After the PS@Fe_3O_4@GO was added into the RhB solution, and reached the adsorption and desorption equilibration, PS@Fe_3O_4@GO was washed with deionised water to remove the unbounded free RhB molecules, using a magnet as a collector. Then the washed PS@Fe_3O_4@GO was re-dispersed in water to characterize the amount of absorbed RhB using UV–vis spectroscopy. The UV–vis spectra of PS@Fe_3O_4@GO before and after loading with RhB were compared as shown in Fig. 5a. As can be seen, a peak at ~553 nm attributed to RhB molecules was observed in the spectrum of washed PS@Fe_3O_4@GO, which demonstrates that RhB molecules were successfully loaded onto PS@Fe_3O_4@GO. The loading quantity of RhB on PS@Fe_3O_4@GO was investigated in different initial concentrations of RhB with respect to the same concentration of PS@Fe_3O_4@GO (2 mg/mL). The adsorption isotherms of RhB on

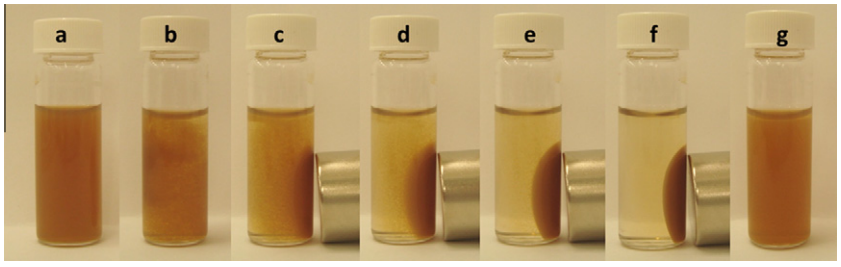

Fig. 4. Photographic images of the behavior of PS@Fe_3O_4@GO composite nanoparticles in the magnetic field under different pH conditions: neutral (a), acidic conditions (pH 3–4) (b–f) and a basic condition (pH 8–9) (g). (b–f) correspond to PS@Fe_3O_4@GO aqueous suspension after 0 s, 15 s, 30 s, 45 s and 60 s, respectively.

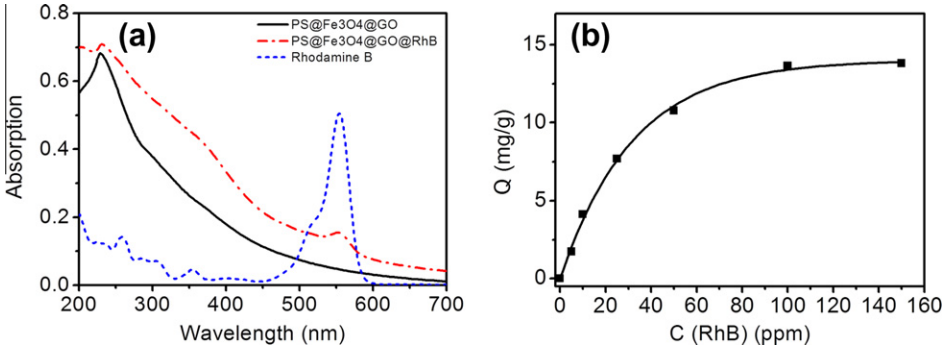

Fig. 5. (a) UV–vis spectra of RhB, PS@Fe_3O_4@GO and PS@Fe_3O_4@GO@RhB. (b) Adsorption isotherms of RhB on PS@Fe_3O_4@GO. m/V (for PS@Fe_3O_4@GO) = 2 mg/mL, C (RhB) initial = 0–150 ppm, T = 293 K.

the PS@Fe_3O_4@GO are shown in Fig. 5b. The maximum adsorption capacity was found to be ~13.8 mg/g. The loading may be attributed to the strong π–π interaction in the form of face-to-face stacking and the hydrogen bonding interaction between GO and RhB [24].

4. Conclusion

Novel PS@Fe_3O_4@GO composite nanoparticles were fabricated using a self-assembly method. Carboxyl functionalized PS latex was used as a template to deposit a layer of Fe_3O_4 nanoparticles and then GO on the spheres. Compared to the previously reported GO@Fe_3O_4 system for possible targeted drug delivery application, the PS@Fe_3O_4@GO composite nanoparticles exhibited a higher loading capacity of Fe_3O_4 nanoparticles, which is favorable for magnetic responsivity to externally applied magnetic field. Moreover, the layered structure retains the efficient surface area of GO to load organic molecules such as RhB. Therefore, the PS@Fe_3O_4@GO nano-spheres have considerable potential in many biomedical applications. Furthermore, PS@Fe_3O_4@GO has a hydrophilic surface and functional groups such as carboxylic groups, which may be further functionalized with other targeting molecules for realizing multi-targeted biological applications.

Appendix A. Supplementary material

Supplementary data associated with this article can be found, in the online version, at http://dx.doi.org/10.1016/j.cej.2012.07.087.

References

[1] C. Lee, X. Wei, J.W. Kysar, J. Hone, Measurement of the elastic properties and intrinsic strength of monolayer graphene, Science 321 (2008) 385–388.
[2] A.A. Balandin, S. Ghosh, W. Bao, I. Calizo, D. Teweldebrhan, F. Miao, C.N. Lau, Superior thermal conductivity of single-layer graphene, Nano Lett. 8 (2008) 902–907.
[3] M.D. Stoller, S. Park, Y.W. Zhang, J. An, R.S. Ruoff, Graphene-based ultracapacitors, Nano Lett. 8 (2008) 3498–3502.
[4] Z. Liu, J.T. Robinson, X. Sun, H. Dai, PEGylated nanographene oxide for delivery of water-insoluble cancer drugs, J. Am. Chem. Soc. 130 (2008) 10876–10877.
[5] K. Yang, L. Hu, X. Ma, S. Ye, L. Cheng, X. Shi, C. Li, Y. Li, Z. Liu, Multimodal imaging guided photothermal therapy using functionalized graphene nanosheets anchored with magnetic nanoparticles, Adv. Mater. 24 (2012) 1868–1872.
[6] X. Ma, H. Tao, K. Yang, L. Feng, L. Cheng, X. Shi, Y. Li, L. Guo, Z. Liu, A functionalized graphene oxide–iron oxide nanocomposite for magnetically targeted drug delivery, photothermal therapy and magnetic resonance imaging, Nano Res. 5 (2012) 199–212.
[7] P. Bradder, S.K. Ling, S. Wang, S. Liu, Dye adsorption on layered graphite oxide, J. Chem. Eng. Data 56 (2010) 138–141.
[8] A.K. Gupta, M. Gupta, Synthesis and surface engineering of iron oxide nanoparticles for biomedical applications, Biomaterials 26 (2005) 3995–4021.
[9] X. Yang, X. Zhang, Y. Ma, Y. Huang, Y. Wang, Y. Chen, Superparamagnetic graphene oxide-Fe_3O_4 nanoparticles hybrid for controlled targeted drug carriers, J. Mater. Chem. 19 (2009) 2710–2714.
[10] Y. Yao, S. Miao, S. Liu, L.P. Ma, H. Sun, S. Wang, Synthesis, characterization, and adsorption properties of magnetic Fe_3O_4@graphene nanocomposite, Chem. Eng. J. 184 (2012) 326–332.
[11] V. Mani, B.V. Chikkaveeraiah, V. Patel, J.S. Gutkind, J.F. Rusling, Ultrasensitive immunosensor for cancer biomarker proteins using gold nanoparticle film electrodes and multienzyme-particle amplification, ACS Nano 3 (2009) 585–594.
[12] R. Massart, Preparation of aqueous magnetic liquids in alkaline and acidic media, Magnetics IEEE Transactions 17 (1981) 1247–1248.
[13] Z. Lu, Y. Qin, J. Fang, J. Sun, J. Li, F. Liu, W. Yang, Monodisperse magnetizable silica composite particles from heteroaggregate of carboxylic polystyrene latex and Fe_3O_4 nanoparticles, Nanotechnology 19 (2008) 055602.
[14] W.S. Hummers, R.E. Offeman, Preparation of graphitic oxide, J. Am. Chem. Soc. 80 (1958) 1339.
[15] M.J. Allen, V.C. Tung, R.B. Kaner, Honeycomb carbon: a review of graphene, Chem. Rev. 110 (2010) 132–145.
[16] C. Gomez-Navarro, R.T. Weitz, A.M. Bittner, M. Scolari, A. Mews, M. Burghard, K. Kern, Electronic transport properties of individual chemically reduced graphene oxide sheets, Nano Lett. 7 (2007) 3499–3503.
[17] S. Stankovich, D.A. Dikin, R.D. Piner, K.A. Kohlhaas, A. Kleinhammes, Y. Jia, Y. Wu, S.T. Nguyen, R.S. Ruoff, Synthesis of graphene-based nanosheets via chemical reduction of exfoliated graphite oxide, Carbon 45 (2007) 1558–1565.
[18] W.L. Zhang, Y.D. Liu, H.J. Choi, Graphene oxide coated core–shell structured polystyrene microspheres and their electrorheological characteristics under applied electric field, J. Mater. Chem. 21 (2011) 6916–6921.
[19] P.H. Wang, C.Y. Pan, Preparation of styrene/acrylic acid copolymer microspheres: polymerization mechanism and carboxyl group distribution, Colloid Polym. Sci. 280 (2002) 152–159.
[20] G.I. Titelman, V. Gelman, S. Bron, R.L. Khalfin, Y. Cohen, H. Bianco-Peled, Characteristics and microstructure of aqueous colloidal dispersions of graphite oxide, Carbon 43 (2005) 641–649.
[21] X.M. Feng, R.M. Li, Y.W. Ma, R.F. Chen, N.E. Shi, Q.L. Fan, W. Huang, One-step electrochemical synthesis of graphene/polyaniline composite film and its applications, Adv. Func. Mater. 21 (2011) 2989–2996.
[22] X. Yang, Y. Wang, X. Huang, Y. Ma, Y. Huang, R. Yang, H. Duan, Y. Chen, Multi-functionalized graphene oxide based anticancer drug-carrier with dual-targeting function and pH-sensitivity, J. Mater. Chem. 21 (2011) 3448–3454.
[23] J. Liu, Q. Zhang, X. Chen, J. Wang, Surface assembly of graphene oxide nanosheets on SiO_2 particles for the selective isolation of hemoglobin, Chem.–Eur. J. 17 (2011) 4864–4870.
[24] H. Zhang, X. Lv, Y. Li, Y. Wang, J. Li, P_{25}-graphene composite as a high performance photocatalyst, ACS Nano 4 (2009) 380–386.